Temperature dependence of the dielectric permittivity of CaF_2, BaF_2 and Al_2O_3: application to the prediction of a temperature-dependent van der Waals surface interaction exerted onto a neighbouring $Cs(8P_{3/2})$ atom

2009 J. Phys.: Condens. Matter 21 255902

(http://iopscience.iop.org/0953-8984/21/25/255902)

IOP Publishing Journal of Physics: Condensed Matter

J. Phys.: Condens. Matter **21** (2009) 255902 (11pp) doi:10.1088/0953-8984/21/25/255902

Temperature dependence of the dielectric permittivity of CaF_2, BaF_2 and Al_2O_3: application to the prediction of a temperature-dependent van der Waals surface interaction exerted onto a neighbouring $Cs(8P_{3/2})$ atom

Thierry Passerat de Silans[1], Isabelle Maurin[1], Pedro Chaves de Souza Segundo[1], Solomon Saltiel[1,2,*], Marie-Pascale Gorza[1], Martial Ducloy[1], Daniel Bloch[1], Domingos de Sousa Meneses[3,4] and Patrick Echegut[3]

[1] Laboratoire de Physique des Lasers, UMR 7538 du CNRS et de l'Université Paris 13, 99 Avenue JB Clément, Villetaneuse, France

[2] Physics Department, Sofia University, 5 J Bourchier Boulevard, 1164 Sofia, Bulgaria

[3] CNRS, UPR 3079 CEMHTI, 1D Avenue de la Recherche Scientifique, F-45071 Orléans Cedex 2, France

[4] Université d'Orléans, Polytech, Avenue du Parc Floral, BP 6749, F-45067 Orléans Cedex 2, France

E-mail: daniel.bloch@univ-paris13.fr

Received 19 December 2008, in final form 16 April 2009
Published 27 May 2009
Online at stacks.iop.org/JPhysCM/21/255902

Abstract

The temperature behaviour in the range 22–500 °C of the dielectric permittivity in the infrared range is investigated for CaF_2, BaF_2 and Al_2O_3 through reflectivity measurements. The dielectric permittivity is retrieved by fitting reflectivity spectra with a model taking into account multiphonon contributions. The results extrapolated from the measurements are applied to predict a temperature-dependent atom–surface van der Waals interaction. We specifically consider as the atom of interest $Cs(8P_{3/2})$, the most relevant virtual couplings of which fall in the range of thermal radiation and are located in the vicinity of the reststrahlen band of fluoride materials.

(Some figures in this article are in colour only in the electronic version)

1. Introduction

Materials that are currently used as optical windows have usually been studied in depth, notably to determine their refractive indices in their transparency regions and the shift of the edges of the transparency region with temperature. In the absorption band, optical investigations of their properties have been commonly performed to get information on their phonon bands, not requiring the same level of accuracy as in common optical applications. However, the optical features of the surface modes, although derived from knowledge of the bulk material, require information on these optical properties within the absorption band. A sensitive tool of these surface properties—benefiting from the high accuracy of atomic physics—is provided by the spectroscopy of an atom in the close vicinity to a surface, through the van der Waals-type long-range surface interaction (see [1] and references

* now deceased.

therein). We have recently addressed [2] the problem of the accuracy of the data existing in the literature for this kind of specific experiment and, in particular, we have shown the high sensitivity of these surface responses to a minor inaccuracy in the bulk properties. This explains that to investigate properties connected to the thermal emissivity of a surface [3–6], an accurate knowledge of the temperature dependence of the optical properties of the material is needed in the thermal infrared range.

In this work, we investigate the temperature dependence of the infrared properties of fluoride crystals CaF_2 and BaF_2. The transparency of these materials extends from UV to mid-IR ranges, and their reststrahlen band, corresponding to a strong absorption, lies in the far-infrared range. Additionally, we also perform measurements on sapphire (Al_2O_3, perpendicular c axis), a well-known optical window material that is considered as a reference for the optical properties and for the planned experiments. To the best of our knowledge, the literature results concerning CaF_2 are limited to ambient temperature [7–9] and 100 K [8] range. For BaF_2 [7, 10, 11], reflectance data were given for the following temperatures: 295, 373, 573 and 773 K. Large discrepancies between published results and their low resolution justify the realization of new measurements.

For Al_2O_3, systematic studies as a function of temperature had already been conducted [12, 13]. The IR behaviour is usually described with the help of several (up to four) phonon modes. However, the experimental findings vary, probably due to variations in the quality of the polishing of the sample, the degree of the impurities and the precision of the measurements.

Our aim in this work is to determine from the knowledge of reflectivity spectra the complex surface response:

$$S(\omega) = \frac{\varepsilon(\omega) - 1}{\varepsilon(\omega) + 1} \tag{1}$$

where $\varepsilon(\omega)$ represents the dielectric function. This research was triggered by an experimental search of the temperature dependence of the atom–surface interaction [4, 5], in which the fundamental effect of vacuum field temperature is susceptible to combine with the temperature dependence of the dense material. As this experiment in progress is performed on the $8P_{3/2}$ level of Cs [6, 14], for which virtual absorptive couplings to Cs ($7D_{3/2}$) and to Cs ($7D_{5/2}$) lie respectively at $\sim$256.4 cm^{-1}($\sim$39 μm) and $\sim$277.8 cm^{-1}($\sim$36 μm), we apply our temperature-dependent evaluations of $S(\omega)$ to the relevant predictions for this specific problem of the influence of the thermal emissivity of materials on the atom–surface interaction. Note that, in principle, extrapolation of surface properties from information from the bulk assumes that the surface is of the same nature as the bulk: let us note that here, surface changes (impurities, crystal reconstruction) occur on a thickness that is truly negligible relative to the thermal infrared wavelengths that we consider. In addition, deriving the bulk properties from a reflectivity measurement implicitly assumes this similar nature of the material in the bulk and at the interface.

This paper is presented in the following way. In section 2, we briefly describe the experimental results with reflectivity spectra as a function of temperature. In section 3, we present the theoretical model [15] of dielectric permittivity that we use to fit the spectra. In section 4, we discuss additional criteria to make individual fittings of a given experimental curve consistent with the expected temperature behaviour, and we provide our estimates of the dielectric permittivity spectra, and of the spectrum of the surface response as a function of temperature. In section 5, we present the results of the calculation of the van der Waals attraction coefficient for Cs($8P_{3/2}$) in front of surfaces of CaF_2, BaF_2 and Al_2O_3 as a function of temperature. By comparing the predictions resulting from various models of permittivity, not limited to our findings, we illustrate why a sensitive knowledge of the temperature-dependent permittivity is required.

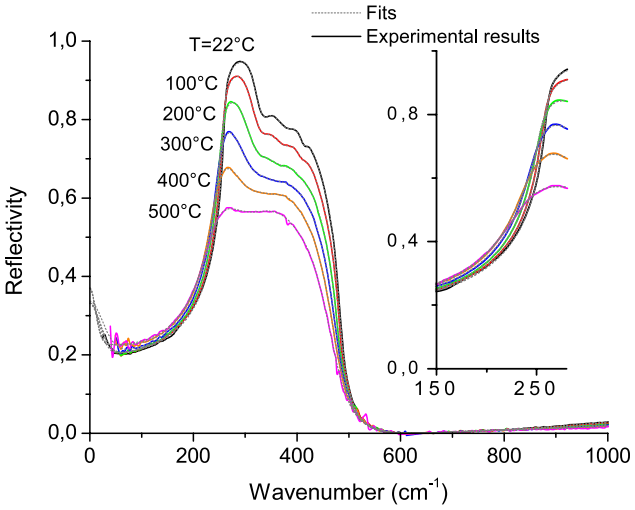

Figure 1. Experimental reflectance spectra of CaF_2 and fits obtained with semi-quantum dielectric function models for sample temperatures between 22 and 500 °C.

2. Experimental details

The samples were optically polished on both sides, with a diameter $\sim$8 mm and a 0.8 mm thickness for CaF_2 and BaF_2, and a 1 mm thickness for Al_2O_3 (with c axis perpendicular to the window). The reflectivity spectra of CaF_2, BaF_2 and Al_2O_3 in the infrared range were acquired with a Bruker infrared Fourier spectrometer (IFS) 113v interferometer for various temperatures ranging between room temperature and 500 °C in steps of 100 °C. The heating was provided by heating a ceramic plate mounted in contact with the rear facet of the sample. The experimental resolution spectrum was $\sim$4 cm^{-1} and the accuracy on the measured reflectivity was $\sim$2–3%.

To extract optical information on the bulk properties of the material, one should note that, as long as the sample is absorbing in the frequency range that is analysed, the reflected intensity only originates in the reflectivity from the input window. Conversely, when the absorption along the sample remains weak, the reflected light should include the reflection from the second window. However, the obtained reflected intensity also combines reflectivity of the sample with the thermal emission of the ceramic hotplate.

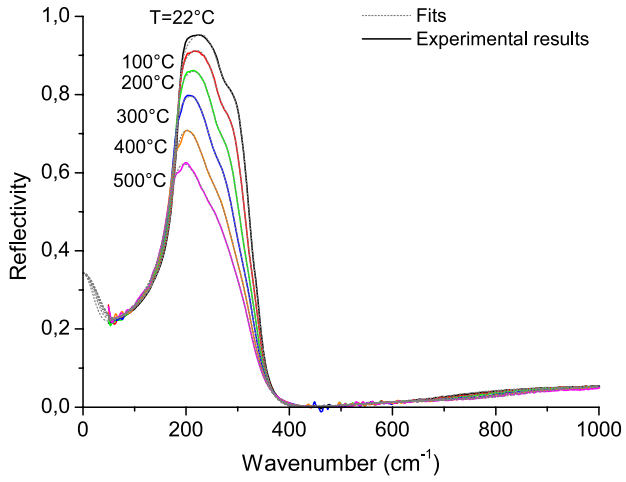

Figure 2. Experimental reflectance spectra of BaF_2 and fits obtained with semi-quantum dielectric function models for sample temperatures between 22 and 500 °C.

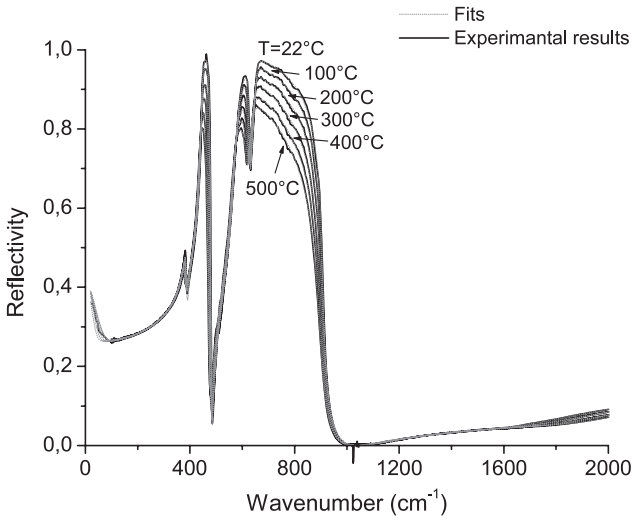

Figure 3. Experimental reflectance spectra of Al_2O_3 and fits obtained with semi-quantum dielectric function models for sample temperatures between 22 and 500 °C.

The measured reflectivity spectra are reported in figures 1–3. For CaF_2, at low temperatures, the spectra exhibit small structures inside the reststrahlen band, which disappear when the temperature increases (see figure 1). These small oscillations, although not consistently mentioned in the literature because of a lower resolution and sensitivity, do not result from interferences nor from an artefact. They were already observed in [7, 8]. Such oscillations are clearly the multiphonon process signature, as explained in [8]. For BaF_2 (see figure 2), we also observe the multiphonon contribution within the reststrahlen band. For Al_2O_3 (see figure 3), the reflectance spectra are more complex and present smaller oscillations also due to multiphonon processes in the reststrahlen region. As a general trend for all these spectra, the sharp edges of the reflectivity get smoother with increasing temperatures.

One also notes on the spectra some apparent oscillations on the wings (50–100 cm^{-1} and 500 cm^{-1} for CaF_2 and BaF_2 or 1000 cm^{-1} for Al_2O_3). They must be attributed to noise: the reflectivity being weak and the detector sensibility low, the signal-to-noise ratio becomes weak.

3. Dielectric constant: theoretical background

In the frame of classical dielectric models [13, 16], the dielectric function ε can be described by

$$\varepsilon(\omega) = \varepsilon_\infty + \sum_j \frac{S_j \Omega_j^2}{\Omega_j^2 - \omega^2 - i\gamma_j\omega} \tag{2}$$

where ε_∞, Ω_j, S_j and γ_j are, respectively, the high-frequency value of the dielectric constant, and the transverse optical wavenumber, the dielectric strength and the damping of the jth phonon. Such a description does not take into account the lattice anharmonicity that makes crystal vibrations interact with the phonon bath in a more complex way: in particular, the damping should not simply be a constant γ_j, but should be highly frequency-dependent, which is due to multiphonon interactions (see [15] and references therein). The effect of this multiphonon interaction was addressed in several models [10, 15]. It can be notably taken into account in an advanced model [15] where γ_j is replaced by a self-energy function $P_j(\omega)$, consisting of a sequence of peaks that are well reproduced by 'extended' Gaussian functions (i.e. with Kramers–Kronig counterparts):

$$\varepsilon(\omega) = \varepsilon_\infty + \sum_j \frac{S_j \Omega_j^2}{\Omega_j^2 - \omega^2 - 2\Omega_j P_j(\omega)} \tag{3}$$

with $P_j(\omega) = \sum_n \tilde{g}_{n,j}(\omega)$:

$$\begin{aligned}\tilde{g}_{n,j}(\omega) = {} & \frac{2A_{n,j}}{\sqrt{\pi}}\left[D\left(\frac{2\sqrt{\mathrm{Ln}(2)}(\omega+\omega_{n,j}^0)}{\gamma_{n,j}}\right)\right. \\ & \left. - D\left(\frac{2\sqrt{\mathrm{Ln}(2)}(\omega-\omega_{n,j}^0)}{\gamma_{n,j}}\right)\right] \\ & + \mathrm{i}A_{n,j}\exp\left(-\frac{4\mathrm{Ln}(2)(\omega-\omega_{n,j}^0)^2}{(\gamma_{n,j})^2}\right) \\ & - \mathrm{i}A_{n,j}\exp\left(-\frac{4\mathrm{Ln}(2)(\omega+\omega_{n,j}^0)^2}{(\gamma_{n,j})^2}\right)\end{aligned} \tag{4}$$

and where $A_{n,j}$, $\omega_{n,j}^0$ and $\gamma_{n,j}$ are, respectively, the amplitude, the location and the damping parameters of Gaussians, and $D(x)$ is the Dawson integral which is given by

$$D(x) = \exp(-x^2)\int_0^x \exp(t^2)\,\mathrm{d}t. \tag{5}$$

Within such a frame, which considerably increases the number of free parameters, a major problem is to identify the right number of parameters, allowing getting an accurate fitting of the experimental spectra, while keeping the number of parameters at a minimum [15]. The objective pursued in section 4 is to extract a unique spectrum of permittivity from the reflectivity data, while finding criteria of consistency relative to the temperature dependence.

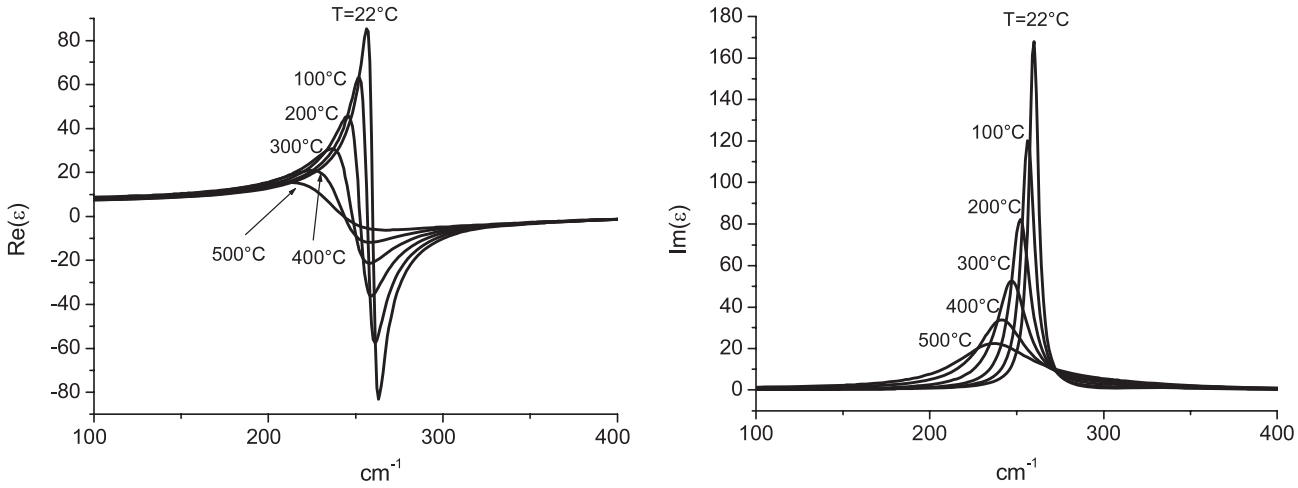

Figure 4. Dielectric constant of CaF_2 (real and imaginary parts) for sample temperatures between 22 and 500 °C.

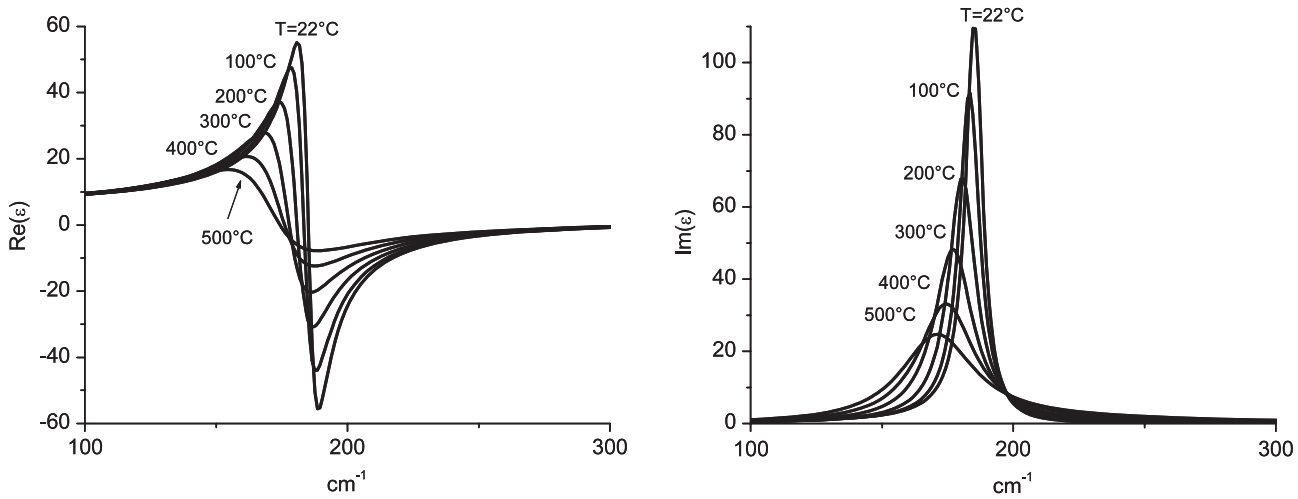

Figure 5. Dielectric constant of BaF_2 (real and imaginary parts) for sample temperatures between 22 and 500 °C.

4. Fitting results and discussion

All the numerical fitting spectra have been obtained with *Focus*, a curve fitting programme developed by one of us (DdSM) that is in free access on the web [17].

In figures 1–3, in which the experimental spectra are reproduced, we have also plotted our best fits obtained on the basis of the semi-quantum model described in section 3. The parameters used for these fits are applied to determine the spectral behaviour of the dielectric permittivity $\varepsilon(\omega)$ (figures 4–6). These parameters are reported in tables 1–3 for CaF_2, BaF_2 and Al_2O_3, respectively, and the complex spectra of self-energy are shown in figures 7–9.

For consistency of the fittings with other known criteria, we have selected fittings for which the extrapolation at zero frequency of the dielectric constant ε_0 is in agreement with the one known in the literature at ambient temperature (i.e. 6.63 for CaF_2 [9], 6.7–7.4 for BaF_2 [11] and 9.395 for Al_2O_3 ordinary ray [18]). We also have tried to impose as much as possible that parameters appearing in the dielectric constants and in the self-energy (see tables 1–3 and figures 4–9) evolve linearly with temperature. Such an *a priori* behaviour can be justified (see, e.g., [19]). Note that, in the absence of such a requirement, which applies to a set of spectra recorded at various temperatures, a single reflectivity spectrum can be equivalently fitted by several systems of parameters, at the expense of the reliability of the extrapolated spectra of permittivity (figures 4–6) or of the surface responses (figures 10–12).

For CaF_2 (figure 1), and as predicted by group theory [20], infrared activity only concerns phonon modes with the T1u symmetry which is triply degenerate. So to fit the infrared spectra and their temperature dependence, a dielectric function model involving a single anharmonic phonon term was used. A rather complex self-energy function was also necessary to reproduce the optical response due to the multiphonon processes, i.e. the numerous small structures appearing within the reflection band. In spite of some apparently erratic variations of the individual parameters with temperature (table 1), these parameters are needed to take care of the evolution of the multiphonon contributions observed around 400 cm^{-1}. Figure 10 shows that the temperature behaviour

Table 1. Parameters of the semi-quantum model used to fit the thermal infrared spectra of CaF_2.

	Temperature (°C)					
	22	100	200	300	400	500
Global parameters						
ε_∞	2.02	2.019	2.07	2.11	2.1	2.16
S_1	4.18	4.04	3.95	3.89	3.83	3.67
Ω_1 (cm^{-1})	272.74	278.17	283.63	288.71	291.76	299.23
Self-energy						
$A_{1,1}$ (cm^{-1})	9.83	8.63	5.01	3.82	14.55	12.12
$\omega^0_{1,1}$ (cm^{-1})	54.67	54.5	54.5	54.5	54.5	54.5
$\gamma_{1,1}$ (cm^{-1})	260.19	245.23	214.99	189.55	167.09	179.98
$A_{2,1}$ (cm^{-1})	8.65	10.15	4.77	7.67	10.88	9.25
$\omega^0_{2,1}$ (cm^{-1})	332.74	328.92	319.06	307.51	307.47	298.43
$\gamma_{2,1}$ (cm^{-1})	31.34	38.81	39.26	51.86	67.18	87.66
$A_{3,1}$ (cm^{-1})	11.145	12.598	14.44	10.27	6.66	4.07
$\omega^0_{3,1}$ (cm^{-1})	370.78	370.35	357.47	345.84	352.88	352.24
$\gamma_{3,1}$ (cm^{-1})	58.39	54.58	89.84	65.17	56.51	79.67
$A_{4,1}$ (cm^{-1})	2.33	3.04	0.995	6.08	3.73	1.74
ω^{41}_0 (cm^{-1})	413.56	408.84	408.99	397.19	398.97	398.97
$\gamma_{4,1}$ (cm^{-1})	18.61	25.91	27.16	77.05	60.76	55.25
$A_{5,1}$ (cm^{-1})	12.95	8.22	5.81	0.97	0.31	0.129
$\omega^0_{5,1}$ (cm^{-1})	448.59	440.498	441.07	443.51	443.78	443.78
$\gamma_{5,1}$ (cm^{-1})	104.74	74.79	80.31	32.76	9.86	6.3
$A_{6,1}$ (cm^{-1})	9.94	23.14	29.56	38.64	46.1	51.45
$\omega^0_{6,1}$ (cm^{-1})	640.11	619.098	625.31	618.89	620.18	621.83
$\gamma_{6,1}$ (cm^{-1})	483.71	436.706	492.69	537.695	602.62	690.66

Table 2. Parameters of the semi-quantum model used to fit the thermal infrared spectra of BaF_2.

	Temperature (°C)					
	22	100	200	300	400	500
Global parameters						
ε_∞	2.12	2.12	2.12	2.11	2.115	2.11
S_1	4.38	4.07	3.799	3.52	3.24	2.99
Ω_1 (cm^{-1})	194.14	202.71	209.42	217.77	226.32	235.02
Self-energy						
$A_{1,1}$ (cm^{-1})	5.13	3.91	2.79	2.078	1.45	0.86
$\omega^0_{1,1}$ (cm^{-1})	132.23	131.107	124.61	133.28	128.533	123.53
$\gamma_{1,1}$ (cm^{-1})	142.04	136.54	136.08	127.26	128.34	124.56
$A_{2,1}$ (cm^{-1})	6.9	5.63	4.64	3.53	4.21	5.24
$\omega^0_{2,1}$ (cm^{-1})	278.48	270.11	260.89	251.44	244.89	243.97
$\gamma_{2,1}$ (cm^{-1})	48.2	40.48	35.17	33.87	46.78	72.15
$A_{3,1}$ (cm^{-1})	13.84	11.23	9.908	8.09	5.42	2.67
$\omega^0_{3,1}$ (cm^{-1})	331.79	326.13	318.63	307.496	295.39	295.89
$\gamma_{3,1}$ (cm^{-1})	46.69	52.66	65.34	80.05	64.18	47.398
$A_{4,1}$ (cm^{-1})	14.97	28.36	37.02	48.67	57.38	64.83
ω^{41}_0 (cm^{-1})	520.53	501.32	494.65	491.41	480.38	481.53
$\gamma_{4,1}$ (cm^{-1})	286.4	321.43	352.42	367.86	385.52	410.35

of the overall shape of the self-energy function, is consistent with the tendency that is expected. The peak amplitude of the corresponding dielectric constant (figure 4) decreases by 82% when the temperature increases from 22 to 500 °C. Simultaneously, the resonance corresponding to the maximum of Im[$\varepsilon(\omega)$] shifts from 260 to 240 cm^{-1}.

Table 3. Parameters of the semi-quantum model used to fit the thermal infrared spectra of Al_2O_3.

	Temperature (°C)					
	22	100	200	300	400	500
ε_∞	3.03	3.013	3.03	2.98	3.019	3.019
S_1	0.42	0.47	0.41	0.49	0.47	0.44
Ω_1 (cm^{-1})	373.86	371	370	359.67	351.66	350.6
$A_{1,1}$ (cm^{-1})	24.41	28.45	26.06	47.79	67.54	62.47
$\omega^0_{1,1}$ (cm^{-1})	199.33	204.6	219.02	219.02	208.88	215.22
$\gamma_{1,1}$ (cm^{-1})	248.99	241.5	229.88	203.74	200.32	196.77
S_2	2.73	2.74	2.63	2.53	2.45	2.41
Ω_2 (cm^{-1})	439.71	436.34	435.06	432.09	429.92	427.39
$A_{1,2}$ (cm^{-1})	5.68	7.87	7.86	8.86	9.49	10.3
$\omega^0_{1,2}$ (cm^{-1})	423.58	419.54	416	413.48	409.06	403.75
$\gamma_{1,2}$ (cm^{-1})	38.51	45.62	59.5	65.28	77.7	93.32
S_3	2.87	2.81	2.87	2.81	2.83	2.82
Ω_3 (cm^{-1})	580.42	582.2	582.98	578.97	581.61	582.95
$A_{1,3}$ (cm^{-1})	1.43	5	11.48	23.67	28.36	29.86
$\omega^0_{1,3}$ (cm^{-1})	371.13	371.61	307.94	354.27	362.12	347.12
$\gamma_{1,3}$ (cm^{-1})	190.22	200.24	237.29	192.02	198.47	206.02
$A_{2,3}$ (cm^{-1})	10.12	9.12	7.86	8.09	5.63	4.75
$\omega^0_{2,3}$ (cm^{-1})	536.83	534.45	526.44	534.32	537.77	526.56
$\gamma_{2,3}$ (cm^{-1})	117.73	108.42	118.29	93.84	79.03	79.42
$A_{3,3}$ (cm^{-1})	15.56	19.17	20.42	25.5	27.59	30
$\omega^0_{3,3}$ (cm^{-1})	914.59	912.06	878.14	839.97	815.08	805.6
$\gamma_{3,3}$ (cm^{-1})	333.25	414.24	418.35	369.58	366.08	362.4
$A_{4,3}$ (cm^{-1})	6.13	6.29	8.99	9.36	15.55	17.81
$\omega^0_{4,3}$ (cm^{-1})	1299.6	1353.68	1298.6	1333.72	1301.19	1294.23
$\gamma_{4,3}$ (cm^{-1})	895.54	953.88	947.96	996.79	927.75	997.607
S_4	0.15	0.15	0.138	0.15	0.17	0.175
Ω_4 (cm^{-1})	638.35	636.59	633.87	628.1	618.72	610.88
$A_{1,4}$ (cm^{-1})	6.77	6.98	7.19	8.78	15.72	22.99
$\omega^0_{1,4}$ (cm^{-1})	640.36	638.2	634.9	619.7	565.2	506.43
$\gamma_{1,4}$ (cm^{-1})	30.03	34.07	35.79	84.38	159.506	233.39

For BaF_2 (figure 2), the fits also involve a single anharmonic phonon term and a self-energy structure to take care of the multiphonon processes. The evolution of the fitting parameters is here clearly monotonic with temperature. The amplitude of the corresponding dielectric constant (figure 5) decreases by 16% when the temperature increases from 22 to 500 °C and the resonance shifts from 185 to 171 cm^{-1}.

For Al_2O_3 (see figure 3), the fit involves four phonon terms, all with their own self-energy functions, but only a single resonance (called S_3 in table 3) exhibits a complex self-energy structure. The amplitude of the corresponding dielectric constant for the main peak decreases by 4.5% when the temperature increases from 22 to 500 °C and the resonance shifts from 443 to 432 cm^{-1} (figure 6).

5. Predictions for the $C_3(T)$ van der Waals coefficient for the interaction between Cs($8P_{1/2}$) and a fluoride window

The long-range atom–surface van der Waals (vW) interaction is a dipole–dipole interaction between the quantum dipole fluctuations of an atom and its electric image induced in the

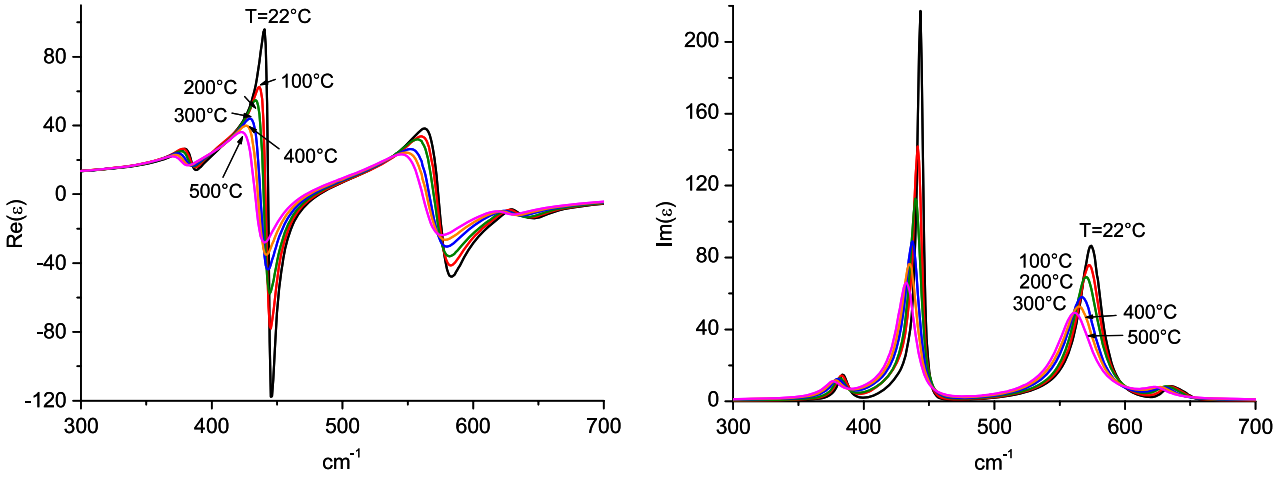

Figure 6. Dielectric constant of Al_2O_3 (real and imaginary parts) for sample temperatures between 22 and 500 °C.

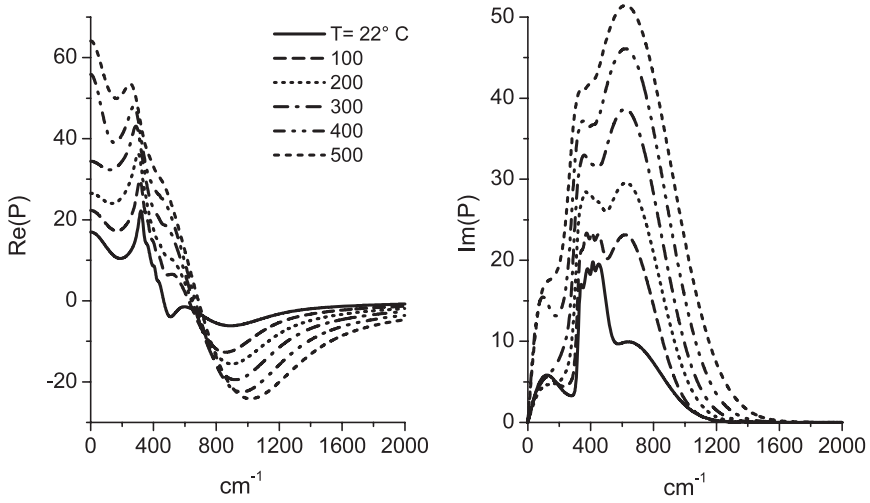

Figure 7. Self-energy $P(\omega)$ (real and imaginary parts) of CaF_2 for sample temperatures between 22 and 500 °C.

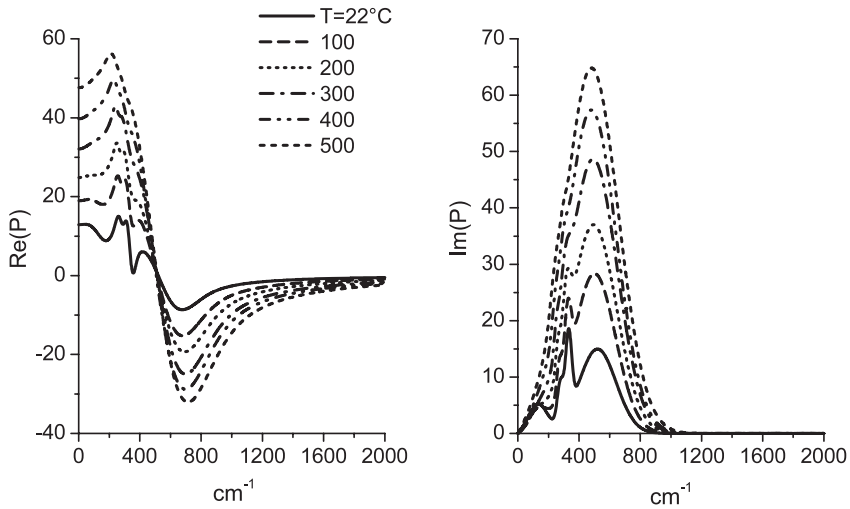

Figure 8. Self-energy $P(\omega)$ (real and imaginary parts) of BaF_2 for sample temperatures between 22 and 500 °C.

surface, so that an atom is submitted to a potential $V(z) = -C_3 z^{-3}$, with z the atom–surface separation and C_3 the coefficient of the van der Waals (vW) interaction (i.e. attraction as long as $C_3 > 0$). The C_3 coefficient is known (for a review, see [21]) to depend notably upon the virtual transitions connecting the atomic level of interest, and upon the surface

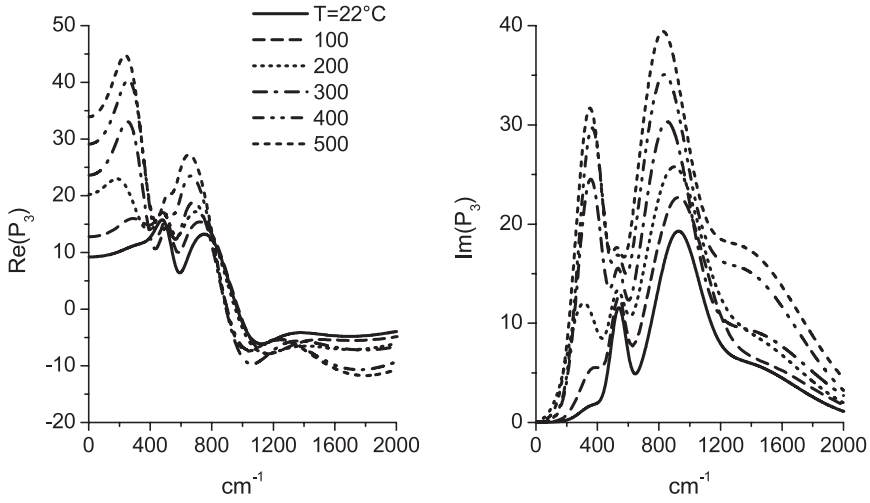

Figure 9. Self-energy $P_3(\omega)$ (real and imaginary parts) of Al_2O_3 (for S_3 resonance only, see table 3) for sample temperatures between 22 and 500 °C.

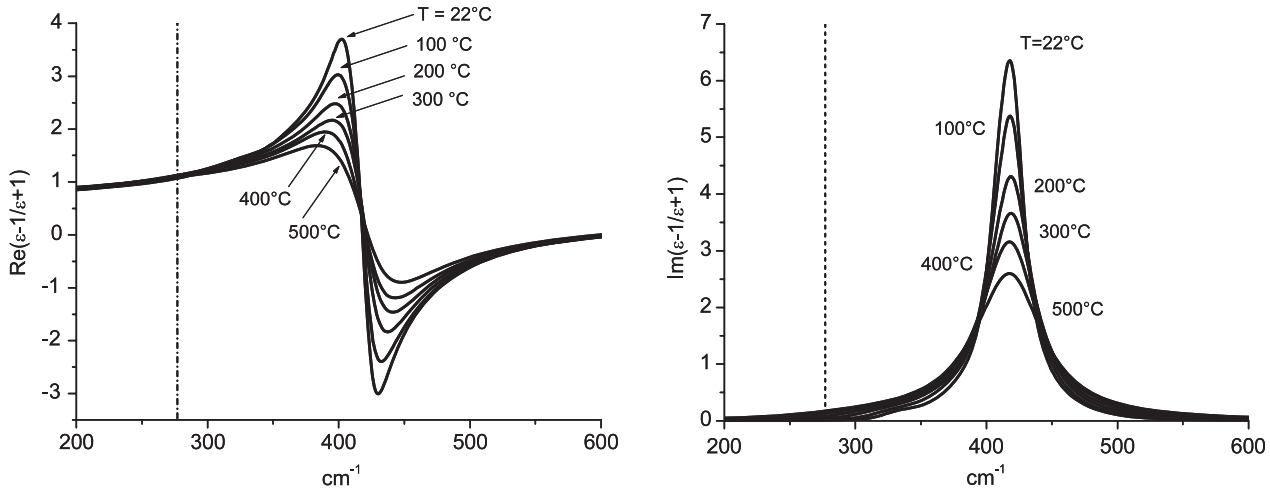

Figure 10. Surface response function $S(\omega)$ of CaF_2 (real and imaginary parts) for sample temperatures between 22 and 500 °C. The virtual atomic absorption of the Cs transition $8P_{3/2} \rightarrow 7D_{3/2}$ is indicated by a vertical dashed line at 277.8 cm^{-1}.

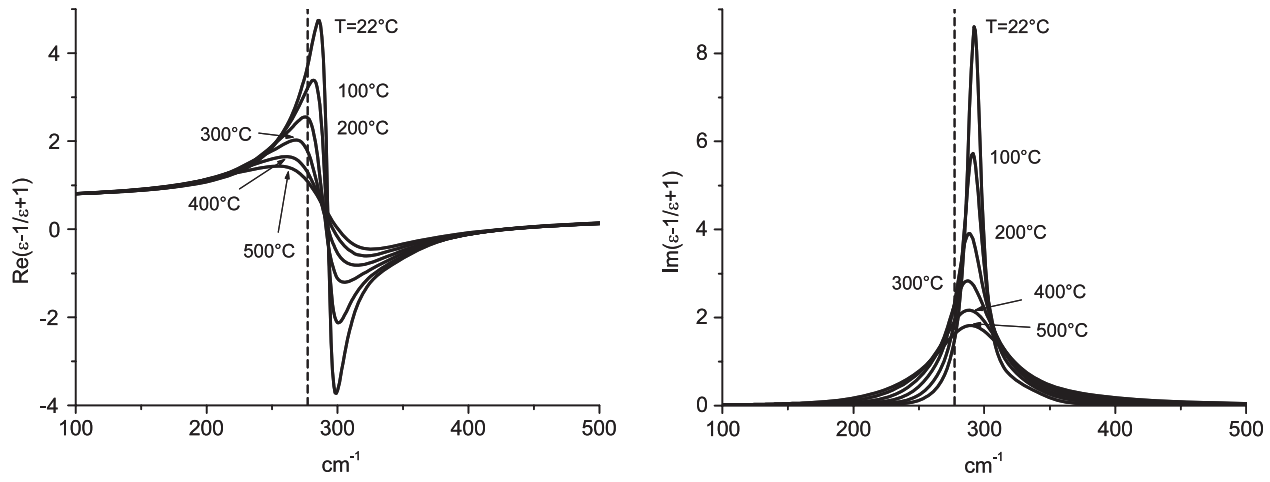

Figure 11. Surface response function $S(\omega)$ of BaF_2 (real and imaginary parts) for sample temperatures between 22 and 500 °C. The virtual atomic absorption of the Cs transition $8P_{3/2} \rightarrow 7D_{3/2}$ is indicated by a vertical dashed line at 277.8 cm^{-1}.

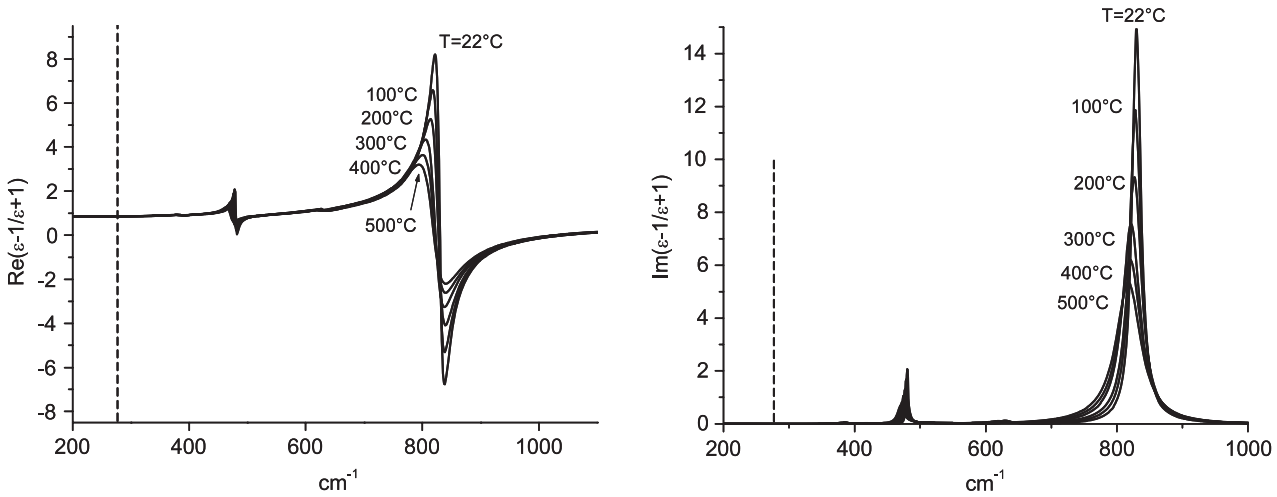

Figure 12. Surface response function $S(\omega)$ of Al_2O_3 (real and imaginary parts) for sample temperatures between 22 and 500 °C. The virtual atomic absorption of the transition $Cs8P_{3/2} \rightarrow 7D_{3/2}$ is indicated by a vertical dashed line at 277.8 cm^{-1}.

resonances, determined from the knowledge of the spectrum of the surface response $S(\omega)$:

$$C_3(|i\rangle) = \Sigma_j r_{ij}(T)\langle i|D|j\rangle^2 \quad (6)$$

with $|i\rangle$ the considered atomic state, D the dipole operator and $r_{ij}(T)$ the dielectric image coefficient. This image coefficient, equal to unity for an ideal electrostatic reflector, depends on the surface response spectrum $S(\omega)$ and on the vacuum temperature.

The theoretical temperature dependence of $r_{ij}(T)$ and hence of $C_3(T)$ was recently analysed in [5] (see notably equations (3.10) and (3.11) of this reference), under the assumption that the temperature of the surrounding vacuum field (i.e. roughly the thermal number of photons) is in equilibrium with that of the dense material. In this approach, the spectrum of the dielectric permittivity is taken as phenomenologically granted. Clearly, to study the evolution over a limited temperature range in [5], and keeping the assumption that the temperature evolution of the vacuum field is relatively decoupled from the details of the spectral modifications of the dense material, the spectrum of dielectric permittivity to be considered should be the one at the relevant temperature.

Below, we apply the results obtained in the preceding sections in order to predict the temperature dependence in the sensitive case of $Cs(8P_{3/2})$, and to compare it with alternative predictions resulting from various modelling of the dielectric permittivity. Indeed, the $8P_{3/2}$ level of Cs, of relatively easy experimental access [6, 14], exhibits major couplings in the thermal infrared range, as recalled in table 4, reproduced from [14]. As already noticed, surface resonances of fluoride materials also fall into the thermal infrared range, so that strong variations of the C_3 coefficient are expected with temperature. In particular, the surface thermal emissivity is susceptible to resonantly couple to a virtual atomic absorption (the frequency position of the most relevant one, at 277.8 cm^{-1} ($\sim$36 μm), is indicated in figures 10–12), opening up the possibility of a vW repulsion above a certain temperature.

Table 4. Contribution of each virtual transition—with transition wavelengths indicated, a minus sign being used for a virtual emission—to the C_3 coefficient for $Cs(8P_{3/2})$, assuming the surface is an ideal reflector [14]. Dominant contributions are printed in bold.

Level (i)	λ (μm)	C_3^i (kHz μm^3)
$5D_{3/2}$	−0.89	<0.01
$5D_{5/2}$	−0.89	0.01
$6D_{3/2}$	−3.12	0.08
$6D_{5/2}$	−3.16	0.71
$7D_{3/2}$	**39.05**	**5.32**
$7D_{5/2}$	**36.09**	**37.78**
$8D_{3/2}$	4.95	0.42
$8D_{5/2}$	**4.92**	**3.70**
$9D_{3/2}$	3.29	0.09
$9D_{5/2}$	3.28	0.80
$10D_{3/2}$	2.72	0.03
$10D_{5/2}$	2.72	0.31
$11D_{3/2}$	2.44	0.02
$11D_{5/2}$	2.43	0.16
$12D_{3/2}$	2.27	0.01
$12D_{5/2}$	2.27	0.09
$6S_{1/2}$	−0.39	0.03
$7S_{1/2}$	−1.38	0.31
$8S_{1/2}$	**−6.78**	**12.07**
$9S_{1/2}$	**8.94**	**11.63**
$10S_{1/2}$	3.99	0.38
$11S_{1/2}$	3.00	0.09
$12S_{1/2}$	2.58	0.04
$C_3 = \sum_i C_3^i = 73.79$ kHz μm^3		

In figures 13–15, we have plotted the predicted C_3 values of $Cs(8P_{3/2})$ as a function of temperature. For purposes of comparison, these values are derived from the formulae obtained in [5] (equations (3.10) and (3.11)) applied with various modellings of permittivity or the dielectric window. Note that, because in equations (3.10) and (3.11) of [5], an analytical expansion of the permittivity is required for the nonresonant term—i.e. the permittivity must be defined for an imaginary frequency—we have actually combined, for the model derived from our measurements, the actual resonant contribution and a nonresonant contribution, gently

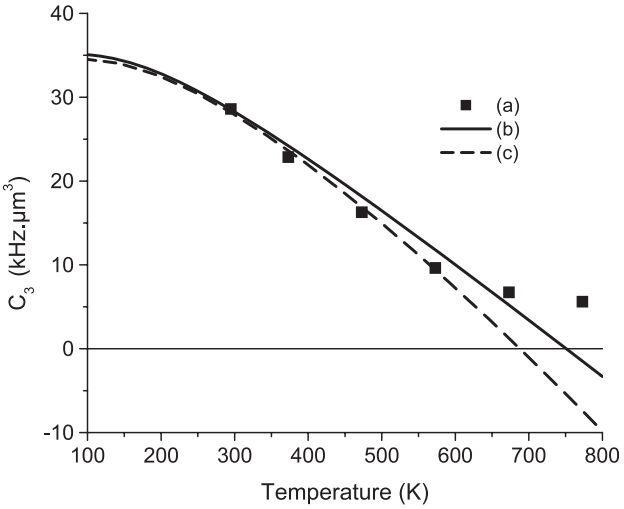

Figure 13. Predicted C_3 vW coefficient for $Cs(8P_{3/2})$ in front of a CaF_2 window as a function of temperature: discrete points (a) CaF_2 permittivity according to the fitting of our temperature-dependent experimental results; curve (b) CaF_2 permittivity according to the room-temperature measurements of [7]; curve (c) CaF_2 permittivity including linear temperature corrections (extrapolated from [8]) to the room-temperature measurements of [7].

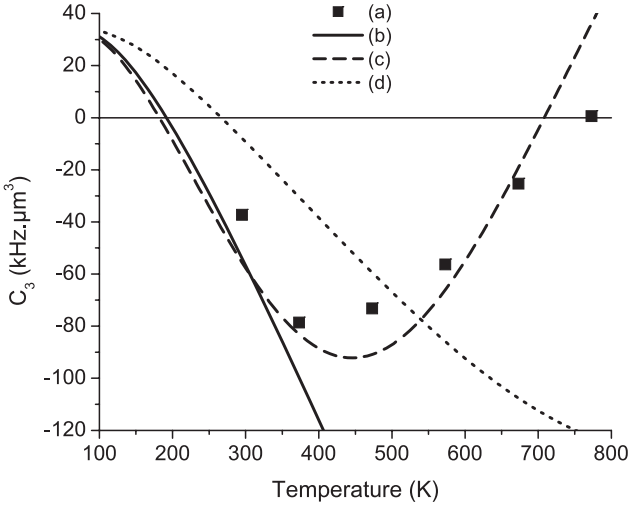

Figure 14. Predicted C_3 vW coefficient for $Cs(8P_{3/2})$ in front of a BaF_2 window as a function of temperature; discrete points (a) BaF_2 permittivity according to the fitting of our temperature-dependent experimental results; curve (b) BaF_2 permittivity according to the room-temperature measurements of [7]; curve (c) BaF_2 permittivity including linear temperature corrections (extrapolated from [8]) to the room-temperature measurements of [7]; curve (d) BaF_2 permittivity including linear temperature corrections (extrapolated from [8]) to the room-temperature measurements of [8].

evolving with temperature, estimated from an elementary classical model for the material: indeed, it is only for the knowledge of the resonant term that an accurate estimate of the permittivity is needed. This comparison includes: (i) the temperature dependence solely resulting from the temperature dependence of the vacuum, the dielectric medium properties being those found (in our experiments) at room temperature; (ii) the discrete evaluations of the C_3 values resulting from our measurements of reflectivity, performed for a discrete set of temperatures and (iii) temperature-linearized models. About this last type of modelling, it is justified in current models in the literature to assume that all temperature dependence of optical parameters of a given material can be linearized [19], once the optical properties of the material were determined for two temperatures. This approach is based on an extended form of the classical oscillator model (cf equation (2)) assuming

$$\varepsilon(\omega, T) = \varepsilon_\infty + \sum_j \frac{S_j(T)\Omega_j^2(T)}{\Omega_j^2(T) - \omega^2 - i\gamma_j(T)\omega} \tag{7}$$

with the temperature dependence of the transverse optical wavenumber Ω_j, of the dielectric strengths, S_j, and of the damping of the jth phonon, linearized in the following form:

$$\begin{aligned} \Omega_j(T) &= \Omega_j(T_0) + a_j[T - T_0] \\ S_j(T) &= S_j(T_0) + b_j[T - T_0] \\ \frac{\gamma_j}{\Omega_j}(T) &= \frac{\gamma_j}{\Omega_j}(T_0) + c_j[T - T_0] \end{aligned} \tag{8}$$

with T_0 a reference temperature, and a_j, b_j and c_j being constant coefficients.

In this modelling, the high-frequency limiting value of the dielectric constant, ε_∞, also exhibits a linear temperature dependence:

$$\varepsilon_\infty(T) = \varepsilon_\infty(T_0) + e[T - T_0] \tag{9}$$

where e is a constant coefficient.

We extrapolate coefficients for linearized temperature dependence from the results of Denham *et al* [8], who measured fluoride crystals' dielectric permittivity at two cold temperatures (100 and ∼300 K) and we find (taking T_0 = 300 K)

for CaF_2 : $a_1 = -0.03\ \text{cm}^{-1}\ \text{K}^{-1}$;

$a_2 = -0.03\ \text{cm}^{-1}\ \text{K}^{-1}$; $b_1 = 0.000\,63\ \text{K}^{-1}$;

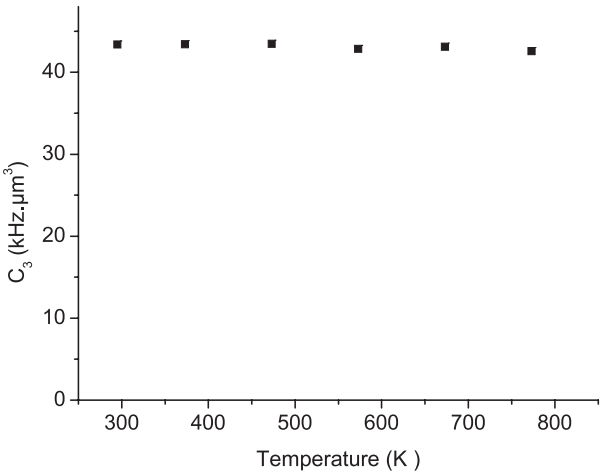

Figure 15. Predicted C_3 vW coefficient for $Cs(8P_{3/2})$ in front of a Al_2O_3 window as a function of temperature: the Al_2O_3 permittivity is according to the fitting of our temperature-dependent experimental results.

$b_2 = 0\ \mathrm{K}^{-1}$; $c_1 = 0.0001\ \mathrm{K}^{-1}$;
$c_2 = 0.000\,25\ \mathrm{K}^{-1}$; $e = -0.000\,03\ \mathrm{K}^{-1}$.

and for BaF_2 : $a_1 = -0.02\ \mathrm{cm}^{-1}\ \mathrm{K}^{-1}$;
$a_2 = -0.035\ \mathrm{cm}^{-1}\ \mathrm{K}^{-1}$; $b_1 = 0.0004\ \mathrm{K}^{-1}$;
$b_2 = 0.000\,13\ \mathrm{K}^{-1}$; $c_1 = 0.0002\ \mathrm{K}^{-1}$;
$c_2 = 0.0005\ \mathrm{K}^{-1}$; $e = -0.000\,045\ \mathrm{K}^{-1}$.

Note that in the modelling of [8]—as in [7]—two phonons are actually obtained, the second phonon with a contribution ten times smaller than the first one, because the multiphonon processes through a self-energy are not considered. Although the experimental results at room temperature in [8] slightly differ from those obtained both in [7] and in our experiments, it can be reasonably assumed that the systematic uncertainties or errors in [8] affect only marginally the extrapolated temperature dependence, so that this linearized temperature behaviour can be applied without inconsistency to the measurements of [7] or [19].

As shown in figure 10, for CaF_2, the atomic transition ($8P_{3/2}$–$7D_{3/2}$) on which the most sensitive temperature effects are expected is located on a wing of the complex response function. This explains that, in figure 13, the temperature behaviour of C_3 is relatively insensitive to the detailed modelling of the CaF_2 response. However, one notes that at the highest temperatures for which we have studied CaF_2, we are not able to predict whether the vW interaction turns out to be repulsive, while this would be a major practical conclusion to be derived in view of the current experiments for CaF_2.

For BaF_2, the atomic transition ($8P_{3/2}$–$7D_{3/2}$) falls in closer resonance with the surface response (figure 11), so that the effects with temperature on the van der Waals coefficients should be very important. Indeed, predictions for the temperature dependence of C_3 radically differ according to the modelling of the BaF_2 response (figure 14). It is clear in particular that the basic model of temperature effects for the vW interaction, although able to predict the fundamental feature of a strong temperature dependence connected to the resonant coupling between the atomic absorption and the thermal emissivity, is far from being sufficient as long as quantitative data are expected. In the refined models for which the temperature dependence of the material properties is also considered, the temperature behaviour for C_3 exhibits strong nonlinear variations: this is because the general effect of broadening of the BaF_2 surface resonance with increasing temperature is susceptible to be enhanced, or counteracted, by the shift of the resonance.

At last, for our 'reference' material Al_2O_3, for which the atomic transitions falling in the thermal infrared ($8P_{3/2}$–$7D_{3/2}$) are out of resonance of the complex response function S (figure 12), the predicted variation of the C_3 coefficient remains marginal (figure 15) in our considered temperature range. The real and imaginary parts at this atomic frequency do not change when the temperature increases.

6. Conclusion

Although fluoride materials are usually considered to be simple and well-known materials, it appears that a precise and consistent fitting of reproducible data require an elaborate procedure. These details, often of a minor importance in most of the applications, can actually lead to dramatic effects when the sharp selectivity of Atomic Physics resonance are considered. Our precise study of temperature dependence should provide a basis for a refined comparison between the theory, and the results of an experiment in progress.

Acknowledgment

The Paris 13 team acknowledges partial support by INTAS South-Caucasus Project (grant 06-1000017-9001).

References

[1] Failache H, Saltiel S, Fichet M, Bloch D and Ducloy M 2003 Resonant coupling in the van der Waals interaction between an excited alkali atom and a dielectric surface: an experimental study via stepwise selective reflection spectroscopy *Eur. Phys. J.* D **23** 237–55
See also Fichet M, Schuller F, Bloch D and Ducloy M 1995 van der Waals interactions between excited states and dipsersive dielectric surfaces *Phys. Rev.* A **51** 1553

[2] Saltiel S, Bloch D and Ducloy M 2006 A tabulation and critical analysis of the wavelength dependent dielectric image coefficient for the interaction exerted by the surface onto a neighbouring excited atom *Opt. Commun.* **265** 220

[3] See e.g. and refs therein Joulain K, Mulet J-P, Marquier F, Carminati R and Greffet J-J 2005 Surface electromagnetic waves thermally excited: radiative heat transfer, coherence properties and Casimir forces revisited in the near field *Surf. Sci. Rep.* **57** 59–112

[4] Dutier G, Hamdi I, Chaves de Souza Segundo P, Yarovitski A, Saltiel S, Sarkisyan D, Papoyan A, Varzhapetyan T, Gorza M-P, Fichet M, Bloch D and Ducloy M 2004 *Coupling of Atoms, Surfaces and Fields in Dielectric Nanocavities Proc. 16th Int. Conf. on Laser Spectroscopy* ed P Hannaford *et al* (Singapore: World Scientific) pp 277–84

[5] Gorza M-P and Ducloy M 2006 van der Waals interactions between atoms and dispersive surfaces at finite temperature *Eur. Phys. J.* D **40** 343–56

[6] Passerat de Silans T, Laliotis A, Romanelli M, Chaves de Souza Segundo P, Maurin I, Bloch D, Ducloy M, Sarkisyan A and Sarkisyan D 2007 Selective reflection spectroscopy of a vapour at a calcium fluoride interface *Ann. Phys. Fr.* **32** 191–4

[7] Kaiser W, Spitzer W G, Kaiser R H and Howarth I E 1962 Infrared properties of CaF_2, SrF_2 and BaF_2 *Phys. Rev.* **127** 1950–4

[8] Denham P, Field G R, Morse P L R and Wilkinson G R 1970 Optical and dielectric properties and lattice dynamics of some fluorite structure ionic crystals *Proc. R. Soc.* A **317** 55–77

[9] Bezuidenhout D F 1991 Calcium fluoride (CaF_2) *Handbook of Optical Constants of Solids II* ed E D Palik (San Diego, CA: Elsevier Academic) pp 815–35

[10] Andersson S K, Thomas M E and Hoffman C 1998 Multiphonon contribution to the reststralhen band of BaF_2 *Infrared Phys. Technol.* **39** 47–54

[11] Thomas M 1998 Barium fluoride (BaF_2) *Handbook of Optical Constants of solids III* ed E D Palik (San Diego, CA: Elsevier Academic) pp 683–99

[12] Gervais F and Piriou B 1974 Anharmonicity in several-polar-mode crystals: adjusting phonon self-energy of LO and TO modes in Al_2O_3 and TiO_2 to infrared reflectivity *J. Phys. C: Solid State Phys.* **7** 2374–86

[13] Gervais F 1983 High-temperature infrared reflectivity spectroscopy by scanning interferometry *Infrared and Millimeter Waves: Electromagnetics Waves* vol 8 (New York: Academic) pp 279–339

[14] Chaves de Souza Segundo P, Hamdi I, Fichet M, Bloch D and Ducloy M 2007 Selective reflection spectroscopy on the UV third-resonance line of Cs: simultaneous probing of a van der Waals atom–surface interaction sensitive to far IR couplings and interatomic collisions *Laser Phys.* **17** 983–92

[15] De Sousa Meneses D, Brun J F, Echegut P and Simon P 2004 Contribution of semi-quantum dielectric function models to the analysis of infrared spectra *Appl. Spectrosc.* **58** 969–74

[16] Puchkov A V, Basov D N and Timusk T 1996 High T_c superconductors: an infrared study *J. Phys.: Condens. Matter* **8** 10049

[17] Focus web site http://crmht.cnrs-orleans.fr/pot/software/focus.html

[18] Tropf W J and Thomas M E 1998 Aluminium oxide (Al_2O_3) *Handbook of Optical constants of solids III* ed E D Palik (San Diego, CA: Elsevier Academic) pp 653–82

[19] Thomas M 1991 Temperature dependence of the complex index of refraction *Handbook of Optical constants of solids II* ed E D Palik (San Diego, CA: Elsevier Academic) pp 177–201

[20] Kroumova E, Aroyo M I, Perez-Mato J M, Kirov A, Capillas C, Ivantchev S and Wondratschek H 2003 Bilbao crystallographic server: useful databases and tools for phase-transition studies *Phase Transit.* **76** 155–70
See also Ganesan S and Burstein E 1965 Selection rules for second order infrared and Raman processes II. Fluorite structure and the interpretation of second order infrared and Raman spectra of CaF_2 *J. Physique* **6** 645–8

[21] Bloch D and Ducloy M 2005 Atom–wall interaction *Advances in Atomic, Molecular and Optical Physics* vol 50 ed B Bederson and H Walther (San Diego, CA: Elsevier Academic) pp 91–156